Nazarbayev University, School of Engineering
Bachelor of Mechanical Engineering

OPTIMUM 2D GEOMETRIES THAT MINIMIZE DRAG FOR LOW REYNOLDS NUMBER FLOW

Final Capstone Project Report

By:
Ilya Lutsenko
Manarbek Serikbay

Principal Supervisor:
Dr.Eng. Konstantinos Kostas
Dr.Eng. Marios Fyrillas

April 2017

Declaration Form

We hereby declare that this report entitled "OPTIMUM 2D GEOMETRIES THAT MINIMIZE DRAG FOR LOW REYNOLDS NUMBER FLOW" is the result of our own project work except for quotations and citations which have been duly acknowledged. We also declare that it has not been previously or concurrently submitted for any other degree at Nazarbayev University.

Name:

Date:

Name:

Date:

Abstract

In this work, a two-dimensional Oseen's approximation for Navier-Stokes equations is to be studied. As the theory applies only to low Reynolds numbers, the results are focused in this region of the flow regime, which is of interest in flows appearing in bioengineering applications. The investigation is performed using a boundary element formulation of the Oseen's equation implemented in Matlab software package. The results are compared with simulations performed in COMSOL software package using a finite element approach for the full Navier-Stokes equations under the assumption of laminar and steady flow. Furthermore, experimental and numerical data from pertinent literature for the flow over a cylinder are used to verify the obtained results. The second part of the project employs the boundary element code in an optimization procedure that aims at drag minimization via body-shape modification with specific area constraints. The optimization results are validated with the aid of finite element simulations in COMSOL.

Content

List of Figures

List of Tables

1. Introduction

A common problem studied in fluid dynamics is the steady flow around a solid object, where the flow's behavior is governed by the Navier-Stokes equations. In the general case, mathematical formulations arising from the full Navier-Stokes description are very complicated and difficult to treat. Therefore, depending on the exact flow conditions, various simplifying approximations are applied, which results in sufficient accuracy.

Essential parameters of dynamic fluid-flow past an immersed body, such as drag and lift coefficients, are of significant importance in many studies. Fluid-flow characteristics are highly dependent on Reynolds number and pertinent applications and research can be split into different areas accordingly: high and medium Reynolds numbers are usually investigated for aerospace or automotive applications, whereas low Reynolds numbers occur mostly in flows investigated for biomedical purposes. The latter field of application has been lately attracting much of researchers' attention as noted in Brody [Brody et. al., 1996]. For instance, flow around blood cells, swimming of microorganisms and targeted drug delivery challenges are all direct applications of low Reynolds number flows. These examples are common demonstrations of highly viscous flows, i.e., flows exhibiting resistance to shape deformation. So, spinning vortices or turbulence is not expected at all, but rather the flow creeps around the obstacle.

In 1911, Carl Wilhelm Oseen criticized Stokes's equation for not being able to solve the 2D creeping flow problem, i.e., the so-called Stoke's paradox [Weisenborn and Mazur, 1984]. Oseen proposed his own extension of the Stoke's flow known as Oseen's equations of motion. Thereby, Oseen's proposal had become a very useful tool to calculate approximately the forces acting on solid objects at low Reynolds numbers, i.e., $Re<<1$. However, it is important to keep in mind that Oseen's equations of motion are not accurate in regions adjacent to body surface. At the same time, there is no standard

range of Reynolds numbers, which can be treated using Oseen's approximation. It is generally recommended to use Oseen's approach at Reynolds numbers much less than one, but there are plenty of works showing successful application of Oseen's equations at Reynolds numbers greater than one. In our research, low Reynolds number flow around a 2D cylinder will be analyzed and the drag coefficient values from different tools will be compared so that the full capability of Oseen's approximation can be established. The main efforts are ultimately focused on:

1. Providing some solid boundaries for the validity of Oseen's approximation and
2. Generating optimum 2D body-shapes that minimize drag in this flow regime.

To demonstrate the importance of low Reynolds number flows and their approximations, some real-life applications are provided: Rosenstein and Leshansky recently studied particles sedimentation in a viscous liquid under the effect of gravity, which is one of the fundamental problems in fluid mechanics [Rosenstein and Leshansky, 2012]. The authors criticize that many works nowadays neglect non-linear effects associated with inertia. In their own research, they analyze the very common phenomenon of multi-particle sedimentation in a fluid using Oseen equations of motion. Furthermore, direct bio-engineering applications of the Oseen's approach drew great attention. Specifically, Brody et. al. emphasized long-term perspectives in the sphere of microfluidic systems [Brody et. al., 1996]. The authors claimed that there is a demand to design a "lab-on-a-chip" concept, which features miniaturized chemical processes in a tiny silicon chip. Within the scope of their work, Brody et. al. focused on analysis of physics behind low Reynolds number flow, which affects the design of micro fabricated devices used in biological processing. Likewise, Resnick and Hopfer addressed bio-engineering application of Oseen's approximation [Resnick and Hopfer, 2007]. By the law of nature, an epithelial cell in an organism comes with a single nonmotile cilium, which appears to perform mechanosensory function in the cell. This feature of the cilium had been profoundly studied and the analysis involved application of Oseen's equations of motion to calculate drag experienced by the cilia.

Considering the aforementioned pertinent results, the main components in this work have as follows:

1) Validation of a Boundary Element Method (BEM) code implemented in MATLAB. The specific code is based on Oseen's equations of motion. The goal is to identify the limits of Oseen's approximation validity, i.e., the Reynolds number range in which the Oseen solution closely follows experimental data. **[Work carried out by Ilya Lutsenko]**

2) Application of Finite Element Method (FEM) using COMSOL Multiphysics [COMSOL Multiphysics user's guide, 2012]. The purpose of FEM's application is to verify the results from BEM. The challenge here will be to create conditions of unbounded fluid flow considering time/resources required for the simulation. **[Work carried out by Manarbek Serikbay]**

3) Comparison of experimental [Tritton, 1959], FEM, and BEM results and establishment of Oseen's capabilities and limitations. **[Work carried out by both Students]**

4) Application of optimization tools, so that optimum 2D geometry that minimize the drag coefficient under specific constraints can be identified. This part requires the parametric definition of the body shape using a small number of parameters: it expresses both the objective function (drag) and constraints as functions of the same set of parameters. Finally, gradient-based and evolutionary algorithms will be employed for getting the optimum. **[Work carried out by both Students]**

Methods used to solve Oseen's equations of motion vary from one paper to another. While some proposed solutions at low Reynolds numbers are not quite accurate due to low order approximations, others are notably precise beyond Reynolds number Re=1[Weisenborn and Mazur, 1983]. Nonetheless, the most compelling argument is that Oseen's equations of motion are efficient at low Reynolds numbers Re<<1. All these considered, our capstone project work tries to determine the full capabilities of Oseen approximation and present a solid range of Reynolds numbers over which Oseen's theory is credible. With respect to possible applications of the theory, the second part of our project focuses on shape optimization targeting 2D body boundaries with minimum drag. The obtained results may find applications in flow problems appearing in biomedical research and generally, when low Reynolds number flows need to be investigated.

2. Background material and Literature review

As it will be presented later in this part of the report, different numerical approaches may yield different ranges for Reynolds number where Oseen approximation is valid. However, all numerical approaches are based on a common principle.

Low Reynolds number flows are defined as the streams within the following region: $Re = \frac{U_0 L}{\nu} \ll 1$. They are also called Stoke's flows or creeping flows. Their main characteristic is that inertial forces are much smaller compared to viscous forces. In our formulation, a non-dimensionalization is performed using the typical Length of the body (L) and the fluid flow velocity U_0: $\bar{x} = \frac{x}{L}, \bar{y} = \frac{y}{L}, \bar{u} = \frac{u}{U_0}, \bar{v} = \frac{v}{U_0}, p = p_0 + \bar{p}P_0$, where *(x, y), (u, v)* are the position and velocity components, respectively and P_0 is the reference pressure, which is equal to $P_0 = (\rho U_0^2)/Re = \mu U_0/L$ for small Reynolds flows [Lagree, 2013]. Boundary conditions in this case are no slip, expressed by $u=0$ and $v=0$ on the body, and $u=1$ and $v=0$ far away from the body, so:

$$\frac{\partial \bar{u}}{\partial \bar{x}} + \frac{\partial \bar{v}}{\partial \bar{y}} = 0 \tag{2.1}$$

$$Re\left(\bar{u}\frac{\partial \bar{u}}{\partial \bar{x}} + \bar{v}\frac{\partial \bar{u}}{\partial \bar{y}}\right) = -\frac{\partial \bar{p}}{\partial \bar{x}} + \left(\frac{\partial^2 \bar{u}}{\partial \bar{x}^2} + \frac{\partial^2 \bar{u}}{\partial \bar{y}^2}\right) \tag{2.2}$$

$$Re\left(\bar{u}\frac{\partial \bar{v}}{\partial \bar{x}} + \bar{v}\frac{\partial \bar{v}}{\partial \bar{y}}\right) = -\frac{\partial \bar{p}}{\partial \bar{y}} + \left(\frac{\partial^2 \bar{v}}{\partial \bar{x}^2} + \frac{\partial^2 \bar{v}}{\partial \bar{y}^2}\right) \tag{2.3}$$

Stoke's flows are considered in the region near the cylinder where left hand side of the Eq.2.2 and Eq.2.3 is infinitesimal compared to right hand side.

Having said that, in two dimensions there is a place for Stoke's paradox, when the flow does not have a solution. This can be shown neglecting left hand side of equations above and introducing stream function: $\psi = LU_0\bar{\psi}$, $\bar{u} = \frac{\partial \bar{\psi}}{\partial \bar{y}}$, and $\bar{v} = -\frac{\partial \bar{\psi}}{\partial \bar{x}}$. Eventually, the solution will be in the form of Eq.2.4, but it does not have a satisfactory solution for a moving flow around an object.

$$\nabla^2 \bar{\psi} = 0 \tag{2.4}$$

Thereby, Oseen's approximation is used in this case as a remedy for the paradox. Integral formulation of Oseen's equations will be presented later.

In addition to isolated analysis of flow regions, there is a solution for the whole region of the flow. It is usually approached by a matched asymptotic expansion method, where separate regions with the corresponding formulas are scrutinized and further combined into one universal equation. The method of matched asymptotic expansions advocates the principle of inner and outer regions. Proudman and Pearson, as pioneers of this method, suggested to divide the region around the cylinder into two separate, but overlapping regions; see Figure 2.1 [Proudman and Pearson, 1957]. The idea is very reasonable: for the inner region, the authors consider Stoke's flow whereas, in the outer region, they assume Oseen's flow.

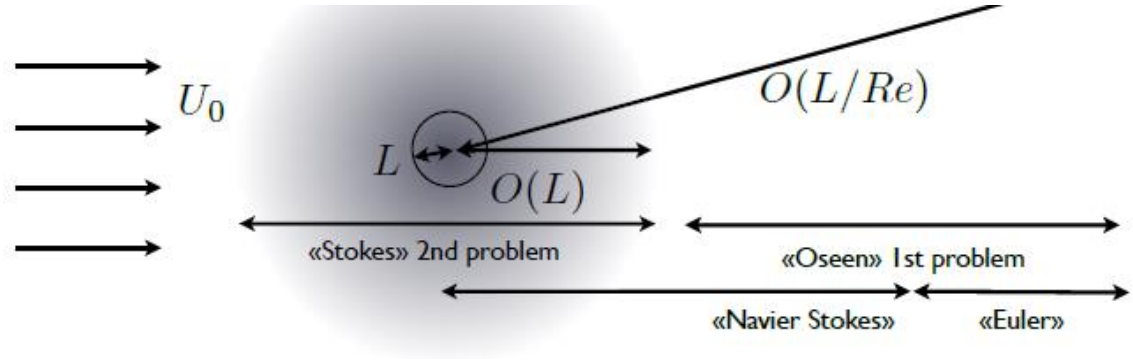

Figure 2.1 Map of matched asymptotic method

Many important research findings and fundamental laws in low Reynolds number flow, discussed above, were deduced before 1980. Therefore, almost all research works performed nowadays rely on some basic principles derived long time ago. In turn, the area of low Reynolds number flow has not been investigated properly yet, e.g. lack of experimental measurements below Reynolds number Re=0.1. Nevertheless, there are research papers that propose a variety of methods to solve Oseen's equations of motion. Each of them differs by complexity, resources required and accuracy of results.

One of the frequently cited experimental results on the flow past a circular cylinder at low Reynolds numbers is coming from D. J. Tritton [Tritton, 1959]. In his experiments, the author measured low air speeds of free convective flow past properly calibrated quartz-fiber anemometers. Such a tool was developed couple of decades before, but had never been used in low Reynolds number experiments. The anemometers attracted Tritton by the fact that they enabled drag measurements at speeds lower than those available for calibration. One end of the quartz-fiber was fixed while the air flow past the free end was viewed through tele-microscope. Applying simple bending moment theory and some assumptions, Tritton ultimately presented the table of drag versus Reynolds number. At low Reynolds numbers, there was a good agreement with experiments performed by other researchers. At the same time, the data agreed satisfactorily with results obtained from different numerical techniques such as Lamb, Kaplun, and others [Tritton, 1959]. A plot of logarithmic values of drag coefficient versus Reynolds number is shown in Figure 2.2.

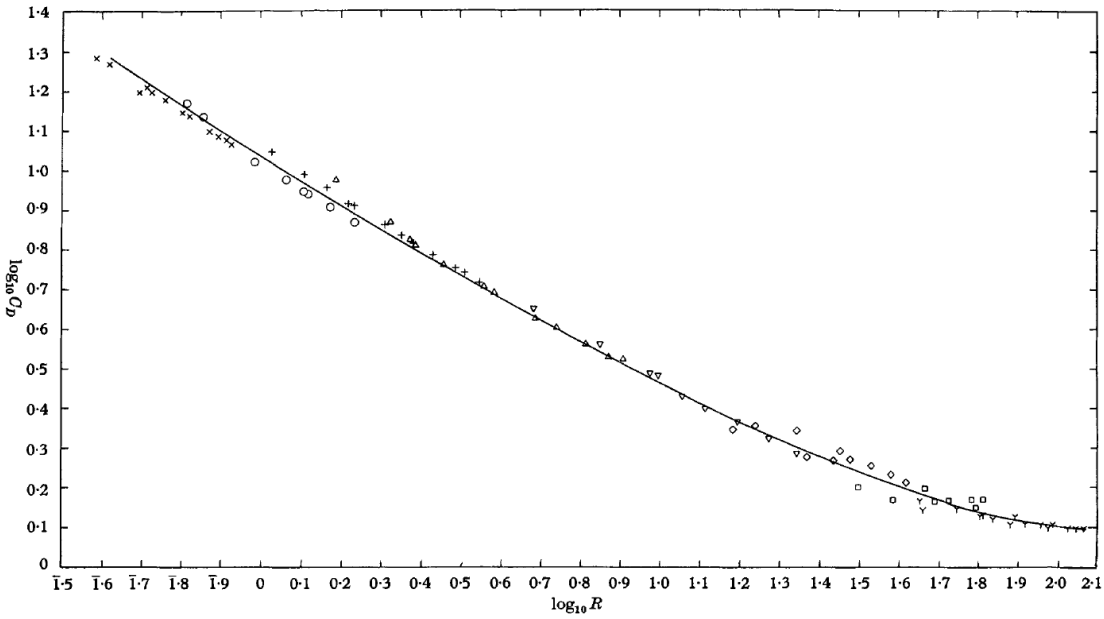

Figure 2.2 Plot of $\log C_D$ against logR showing all observations listed in Tritton's experiments. The line is an estimated mean of readings from different fibers.

Contemporary research papers on Oseen's flow propose numerical solutions of different complexity and accuracy. Bush presented a boundary element formulation of Oseen's equations with quite good accuracy compared to full Navier-Stokes equations [Bush, 1983]. However, the method was limited to very low Reynolds number problems *Re<<1*. Another numerical method worth mentioning is the work by Yano and Kieda. The authors developed a discrete singularity method with the least squares criterion for the 2D potential flow problem [Yano and Kieda, 1980]. Simply speaking, the interior of the obstacle is discretized into so-called *Oseenlets* and then a least squares criterion is applied. The method demonstrated that in the case of a circular cylinder, Oseen's equations of motion are valid even at Reynolds numbers greater than one. Yano and Kieda compared their results with empirical data presented by Tritton and found out that values are relatively close for Reynolds number Re < 4 [Yano and Kieda, 1980]. In turn, Weisenborn and Mazur too compared their method with Tritton's experimental data. Their approach does not require explicit knowledge of the velocity and pressure fields as Yano and Kieda's model does, but rather the model uses a method of induced forces. The authors assert that the approach is effective up to Reynolds number Re=10 [Weisenborn and Mazur, 1984].

3. Methods and tools description

3.1. Integral formulation of the Oseen problem in 2D

Derivation of integral equations for Oseen problem has been studied very extensively in many research papers, e.g. Olmstead and Gautesen work [Olmstead and Gautesen, 1976]. Consider Oseen's equations below:

$$\frac{\partial v_k}{\partial x_k} = 0,\ Re * \alpha_k \frac{\partial v_i}{\partial x_k} = -\frac{\partial p}{\partial x_i} + \Delta v_i \tag{3.1.1}$$

with the following boundary conditions: $v_i = 0$ on the body surface, $v_i \to \alpha_i$ and $p \to 0$ at infinity. Re from now on is denoted by R for simplicity.

There is a direct way to solve coupled partial differential equations, Eq. (3.1.1). However, Olmstead and Gautesen proposed a fundamental solution of the Oseen's equations, which involves the velocity tensor and pressure vector. The principle behind this fundamental approach is underpinned by a theory of point forces. A unit point force produces coupled velocity and pressure, which corresponds to vector-scalar pair (E_{1i}, e_1), (E_{2i}, e_2) [Olmstead and Gautesen, 1976]. Fundamental equations are demonstrated in Eq. (3.1.2), where Kronecker delta δ_{ij} and delta function $\delta(x - \xi)$ are involved:

$$\frac{\partial E_{ik}}{\partial x_k} = 0,\ R\alpha_k \frac{\partial E_{ij}}{\partial x_k} = -\frac{\partial e_i}{\partial x_j} + \Delta E_{ij} + \delta_{ij}\delta(x - \xi) \tag{3.1.2}$$

Then, the solutions for velocity and pressure become:

$$\boldsymbol{v}(\boldsymbol{x}) = \boldsymbol{\alpha} + \int \boldsymbol{E}(\boldsymbol{x} - \boldsymbol{\xi}; \boldsymbol{R}) * \boldsymbol{t}(\boldsymbol{\xi}) dS \tag{3.1.3}$$

$$p(x) = \int \boldsymbol{e}(\boldsymbol{x} - \boldsymbol{\xi}; \boldsymbol{R}) * \boldsymbol{t}(\boldsymbol{\xi}) dS, \quad (3.1.4)$$

where $\boldsymbol{x} = \{x; y\}$ is a point in the flow, $\boldsymbol{\xi} = \{\xi; \eta\}$ is a point on the surface of the immersed body, $\boldsymbol{E}$ is a velocity tensor, $\boldsymbol{e}$ is a pressure vector, and $\boldsymbol{\alpha} = \{1,0\}$ is a free flow velocity vector.

In turn, the integration is applied over the surface area of the obstacle and local stress vector t= $\{t_i\}$ on the surface is expressed by $\boldsymbol{t_i}(\boldsymbol{x}) = -p\boldsymbol{n_i} + (\frac{\partial v_i}{\partial x_k} + \frac{\partial v_k}{\partial x_i})\boldsymbol{n_k}$. In simple words, the local stress vector is an intensity of distribution of the point forces over the surface of a body, i.e., points with $v = 0$.

By introducing new notations such as $E_{ij}(x - \xi; R) = V_{ij}(x - \xi, y - \eta; R)$, $e_i(x - \xi; R) = P_i(x - \xi, y - \eta)$ and $t_i(\xi) = \tau_1(s)$, the general expressions for 2D velocity and pressure becomes:

$$v_i(x, y) = \alpha_i + \int V_{i1}(x - \xi, y - \eta; R)\tau_1(s)\, ds + \int V_{i2}(x - \xi, y - \eta; R)\tau_2(s)\, ds \quad (3.1.5)$$

$$p(x, y) = \int P_1(x - \xi, y - \eta)\tau_1 ds + \int P_2(x - \xi, y - \eta)\tau_2 ds \quad (3.1.6)$$

Then, solving for the unknowns in Eq. (3.1.5) and Eq. (3.1.6), Olmstead and Gautesen used the velocity tensor and pressure vector definitions shown below [Olmstead and Gautesen, 1976]:

$$E_{ij}(x - \xi; R) = \left(\delta_{ij}\Delta - \frac{\partial^2}{\partial x_i \partial x_j}\right) * \left(-\frac{1}{2\pi R}\int_0^{\xi_1 - x_1} \left[\log r' + e^{-\frac{R\mu}{2}} K_0\left(\frac{1}{2}|R|r'\right)\right] d\mu + \right.$$
$$\left. + \frac{1}{4\pi}\int_0^{\xi_2 - x_2} (\xi_2 - x_2 - \mu) K_0\left(\frac{1}{2}|R||\mu|\right) d\mu\right) \quad (3.1.7)$$

$$e_i(x-\xi;R) = -\frac{\partial}{\partial x_i}\left(\Delta - R\frac{\partial}{\partial x_1}\right) * (-\frac{1}{2\pi R}\int_0^{\xi_1-x_1}\left[\log r' + e^{-\frac{R\mu}{2}}K_0\left(\frac{1}{2}|R|r'\right)\right]d\mu + \\ + \frac{1}{4\pi}\int_0^{\xi_2-x_2}(\xi_2 - x_2 - \mu)K_0\left(\frac{1}{2}|R||\mu|\right)d\mu) \quad (3.1.8)$$

where $r = |x-\xi|$, $r' = [\mu^2 + (\xi_2 - x_2)^2]^{\frac{1}{2}}$, and K_0 is a modified Bessel function.

Thereby, the authors derived the following five equations:

$$4\pi V_{11}(x-\xi, y-\eta; R) = e^{R(x-\xi)/2}[K_0\left(\frac{1}{2}|R|r\right) + \frac{R(x-\xi)}{|R|r}K_1\left(\frac{1}{2}|R|r\right)] - \frac{x-\xi}{\frac{1}{2}Rr^2} \quad (3.1.9)$$

$$4\pi V_{12}(x-\xi, y-\eta; R) = 4\pi V_{21}(x-\xi, y-\eta; R) \\ = e^{R(x-\xi)/2}\frac{R(y-\eta)}{|R|r}K_1\left(\frac{1}{2}|R|r\right) - \frac{y-\eta}{\frac{1}{2}Rr^2} \quad (3.1.10)$$

$$4\pi V_{22}(x-\xi, y-\eta; R) = e^{R(x-\xi)/2}[K_0\left(\frac{1}{2}|R|r\right) + \frac{R(x-\xi)}{|R|r}K_1\left(\frac{1}{2}|R|r\right)] - \frac{x-\xi}{\frac{1}{2}Rr^2} \quad (3.1.11)$$

$$2\pi P_1(x-\xi, y-\eta) = -\frac{x-\xi}{r^2} \quad (3.1.12)$$

$$2\pi P_2(x-\xi, y-\eta) = -\frac{y-\eta}{r^2} \quad (3.1.13)$$

where $= [(x-\xi)^2 + (y-\eta)^2]^{\frac{1}{2}}$.

Finally, for determining the stress vector components, we consider an arbitrary point $\boldsymbol{\xi}' = \{\xi', \eta'\}$ on the plain curve Γ and get:

$$-\int V_{11}(\xi'-\xi, \eta'-\eta; R)\tau_1(s)ds - \int V_{12}(\xi'-\xi, \eta'-\eta; R)\tau_2(s)ds = 1 \quad (3.1.14)$$

$$-\int V_{12}(\xi'-\xi, \eta'-\eta; R)\tau_1(s)ds - \int V_{22}(\xi'-\xi, \eta'-\eta; R)\tau_2(s)ds = 0 \quad (3.1.15)$$

Solving the provided equations assists in obtaining drag and lift values, whereas derivation of corresponding coefficients is a straight-forward procedure.

3.2. Matlab

One of the software packages used in our project is MATLAB. The code developed is divided into several parts. First of all, a part is devoted for the construction of body shapes using the NURBS toolbox (Non-Uniform Rational Basis Spline). This mathematical representation is usually employed for generating curves, surfaces and solid models in modern CAD systems. NURBS parametric representations can be used to exactly represent conic sections and, at the same time, both B-Spline and Bézier geometrical entities may be modelled with NURBS. Shape definition and control is mainly carried out with the notion of control points.

In the special case of a simple Bézier curve, i.e., a Bézier curve composed by a single polynomial segment, we will have n+1 control points, from P_0 to P_n, where n is the degree of the curve, while P_0 and P_n coincide with curve's end points. Intermediate control points do not usually lie on the curve. A point on the curve is computed as a convex combination of the curve's control points. As an example, a simple quadratic Bezier curve can be defined as follows:

$$B(t) = (1-t)[(1-t)P_0 + tP_1] + t[(1-t)P_1 + tP_2] \qquad (3.2.1)$$

where $0 \leq t \leq 1$

The construction of the curve (red curve) as parameter t moves in [0,1] is depicted in Figure 3.2.1.

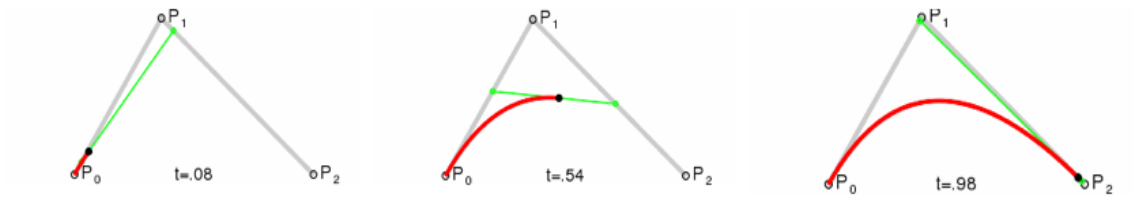

Figure 3.2.1. Quadratic Bézier curve

Simple cubic Bézier curves are used in our modelling as greater shape flexibility is allowed by a cubic polynomial. A cubic Bézier curve uses 4 control points and can be defined as in Eq.3.2.2 with respect to its parameter t.

$$B(t) = (1-t)^3 P_0 + 3(1-t)^2 t P_1 + 3(1-t) t^2 P_2 + t^3 P_3 \qquad (3.2.2)$$

where $0 \leq t \leq 1$

The generation of a simple cubic Bézier curve is depicted in Figure 3.2.2, where P_0, P_1, P_2 and P_3 are its control points.

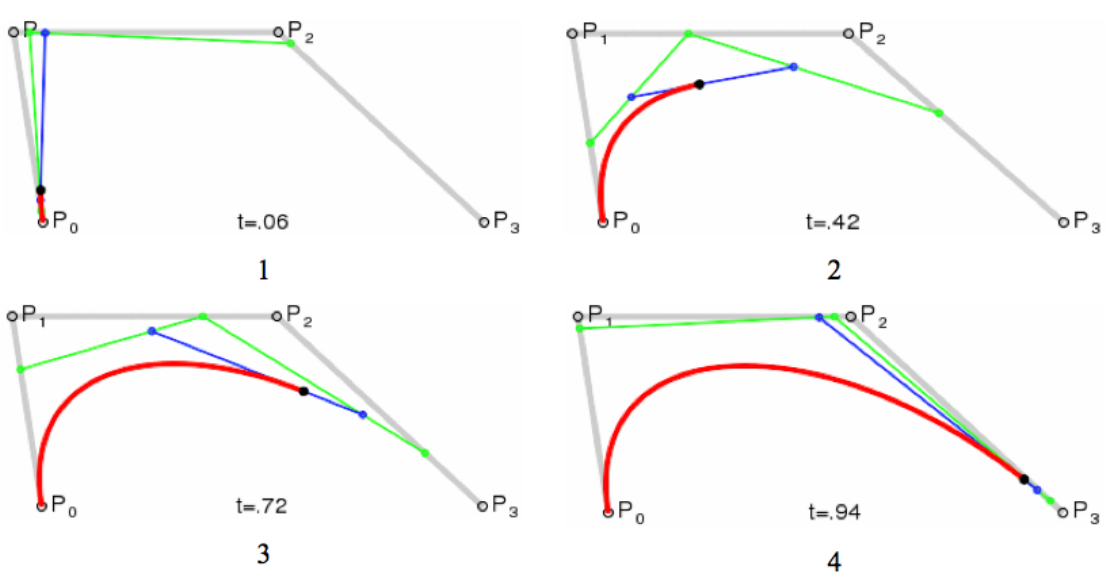

Figure 3.2.2. Cubic Bézier curve

As our project studies were concentrated on a cylinder drag investigation with non-dimensional diameter D=1, this shape will be our input geometry for devising a parametric spline model, which will be further used in shape optimization. The cylinder, i.e., circle in our 2D case, can be divided into four equal 90^o arcs and each arc will be

approximated by a separate simple cubic Bèzier Curve. The characteristic length, i.e., the circle's diameter or generally the shape's max length, will be fixed to 1 unit allowing a fixed Reynold's number and direct comparisons of Drag Coefficients. The general shape is parameterized using the following parameters: B, X_b, a and a_2. All of them are depicted on Figure 3.2.3 and will be used in shape optimization.

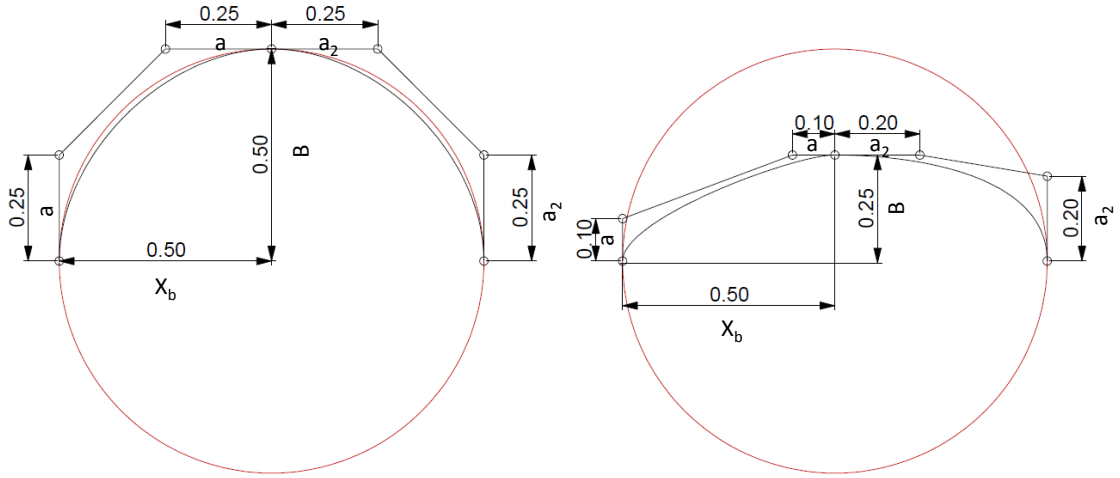

Figure 3.2.3. NURBS generated shape example with the main optimization parameters a, a2, X_b, B and initial input cylinder with diameter D

For performing this shape optimization, several important decisions need to be made. First of all, it was decided to make the final shape symmetric only about the horizontal axis, so only half of the shape needs to be defined, since the remaining part will be its symmetric with respect to the horizontal axis. Secondly, it was assumed that sharp edges are undesired features for the investigation with the available coding precision, as usually similar geometries result in calculation errors. Therefore, a and a_2 values are set to be always greater or equal to 10% of B, making sure that leading and trailing edges are locally flat. Based on the following assumptions and using non-dimensionalized values of B, X_b, a and a_2 we can define the four control points for each of the two spline segments corresponding to the upper part of our shape.

After shape generation an area calculation function was introduced for estimating the shape's interior area. The calculation is performed using an adaptive quadrature method that can always satisfy the required precision. In successive optimization steps this function is used for the definition of the area constraint. Specifically, the generated shape's area is required to be equal to that of circular disc of diameter D=1.

Lately, the forces acting on the generated shape are studied. For this purpose DragCoefKK.m file is created. It builds a shape to be studied with NURBS toolbox and calculates drag and lift coefficients for that shape. In turn, the methodology for calculating drag and lift forces is implemented in BEF.m file. It initially estimates the required number of elements and assigns the unknown physical quantity at the midpoint of element. Afterwards influence matrices are determined employing Gauss-Kronrod quadrature integration method from quadgkmmf.m file. With the obtained influence matrices tensor vectors are figured out. The mentioned tensor vectors are then immediately transferred for Drag and Lift forces computation multiplying their values by the length of impacted object surface. From Drag and Lift forces corresponding resistance coefficients can be directly calculated, which are the required findings of this part.

Finally, with the aid of the previously mentioned components, the optimization can be executed. The main aim of the optimization is to achieve the least drag with a minimum deviation between the optimized shape area and the initial circular disc area. The process is performed using two different optimization algorithms, Fmincon and GA; both provided by MATLAB software package. Fmincon employs by a default a SQP (Sequential Quadratic Programming) based method for finding the minimum of a constrained nonlinear multivariable function. It's a fast deterministic method, which however, might return wrong results in case of objective functions with several local minima. Hence, in such cases the result will be highly dependent on the method's starting point. GA method is a Genetic Algorithm implementation, which is more preferable in terms of final results robustness, but requires significantly more

calculation time and will only provide an approximation of the final minimizer. Both methods were executed multiple times to ensure proper execution and validate the results. Furthermore, a detailed log was created for each run recording all method iterations, the shapes that have been generated and all intermediate results. These logs can be checked manually to track errors or spot problems.

3.3. COMSOL

In our project we have used COMSOL Multiphysics 4.4 as the finite element method solver. COMSOL Multiphysics is a powerful software platform that is designed for modelling and solving different kinds of scientific and engineering problems. According to the software user's guide (2012), a user-friendly desktop environment is provided with a Model Builder component that exploits the full functionality potential of the tool. The software also allows the setup and computation of problems that involve multiple physical phenomena, which is extremely helpful in solving complex engineering problems. Like most FEM tools, COMSOL does not require in-depth knowledge of the underlying math or numerical implementations and has been used extensively in many areas such as acoustics, fluid dynamics, heat transfer, microfluidics, electromagnetics and others.

Within the scope of this capstone project, only 2D Laminar flow analysis is used. The simulation in COMSOL obeys the full Navier-Stokes equations for steady and incompressible Newtonian fluid:

$$\rho \nabla . u = 0 \tag{3.3.1}$$

$$\rho (u . \nabla) u = \nabla . [-pI + \mu(\nabla u + (\nabla u)T)] + F \tag{3.3.2}$$

In designing a valid simulation, it was very important to create conditions of an

unbounded fluid flow. Therefore, the general domain size is much larger than the characteristic length of a cylinder, i.e., while radius of the cylinder is R=0.5, the length and width of an air tunnel is L=900R and W=300R respectively. All the parameters are non-dimensionalized to simplify the analysis. Also, for reducing the computational time and resources required for such a large domain, it was decided to apply user-controlled meshing. Using specific Boolean operator, i.e., partitioning, the domain was divided into three smaller parts. Normal mesh size was imposed onto the domain far from the cylinder, while the domain around the cylinder was meshed with extra and extremely fine mesh. Refer to Tables 3.3.1 and 3.3.2 for parameters and boundary conditions of the simulation.

Table 3.3.1 Simulation parameters

Global parameter	**Value**
Cylinder radius	$R = 0.5$
Length of the domain	$L = 900R$
Width of the domain	$W = 300R$
Fluid material-air	Density, $rho - 1$; dynamic viscosity, $\mu = 1/Rey$
Flow velocity	$Uin = 1$

Table 3.3.2 Simulation boundary conditions

Boundary condition	**Value**
Inlet(laminar inflow)	$Uaverage = Uin, Lentrance = 1m.$
Outlet(pressure condition)	$p_0 = 0\ Pa$ (suppress backflow)
Symmetry	Top and bottom domain (rectangle) boundaries

It is worth to note that Drag is computed using a predefined variable in COMSOL. The software proposes the variable spf.K_stressx and line integration technique in calculating for the Drag force.

Simple 2D laminar airflow simulation was run on COMSOL. As mentioned in previous section, the main challenge was to select a domain of suitable size, such that the fluid is not bounded. Simply speaking, it was desired to have gradual variation of velocity contour until there is a color uniformity (corresponding to the velocity) everywhere in the domain. Then the domain was partitioned into three parts. Mesh size increases outwards from the cylinder as shown below in Table 3.3.3, Figure 3.3.1 and Figure 3.3.2:

Table 3.3.3 Domains and corresponding mesh sizes

Domain	Minimum element size	Growth rate	Maximum element size
1	0,004	1,1	0,5
2	0,06	1,3	0,7
3	0.06	1,3	3

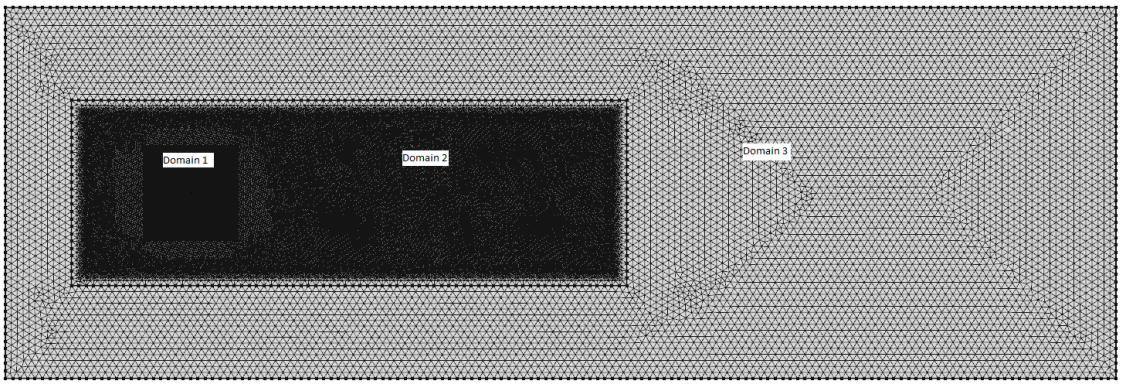

Figure 3.3.1 Mapped computational domain

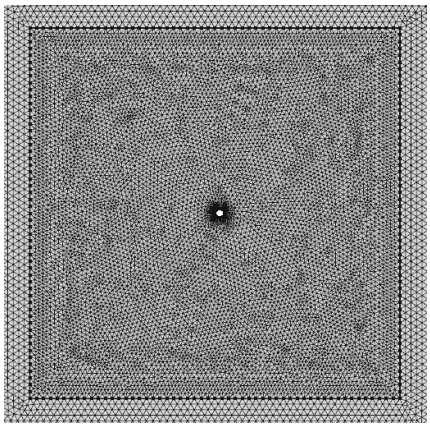

Figure 3.3.2 Enlarged view of Domain 1.

Validation of Oseen's approximation in the present study is performed using Tritton's empirical data [Tritton, 1959]. Thereby, COMSOL simulations are launched starting from Reynolds number Re=0.387. A typical plot of velocity and pressure at Re=0.387 is shown below; other velocity/pressure contour plots can be found in appendix. It should also be mentioned that all simulations were carried out on a PC with an Intel® Core™ i5-4690 CPU @ 3.50GHz with 8.00GB RAM and a 64-bit Windows Operating System.

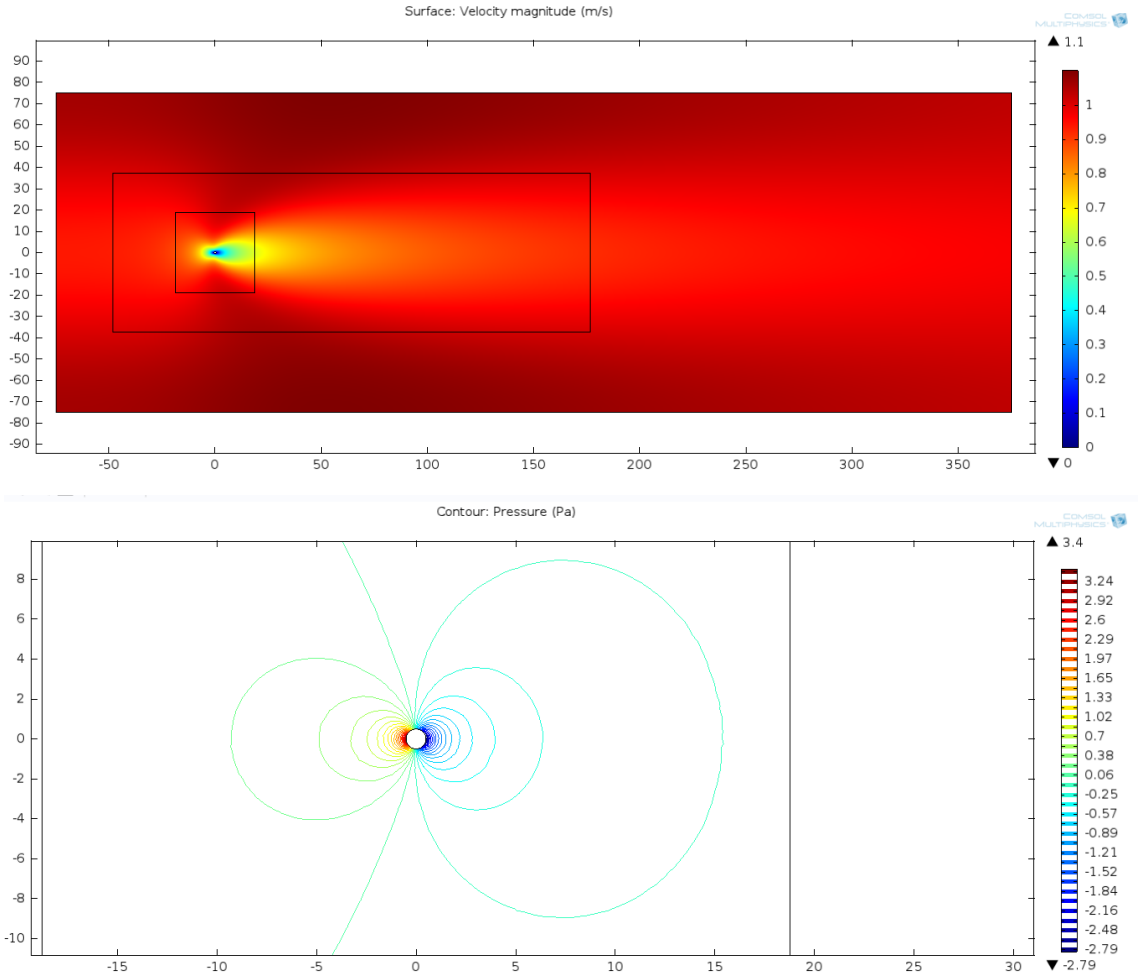

Figure 3.3.3 Velocity and pressure contours around the cylinder at Reynolds number Re=0.387

4. Results and discussions

4.1 Validation of Oseen's approximation

In this part of the report, drag coefficient values from several tools and sources are compared. Whereas main components of the report are demonstrated in Figure 4.1.1, all the results are summarized in Table 4.1.1

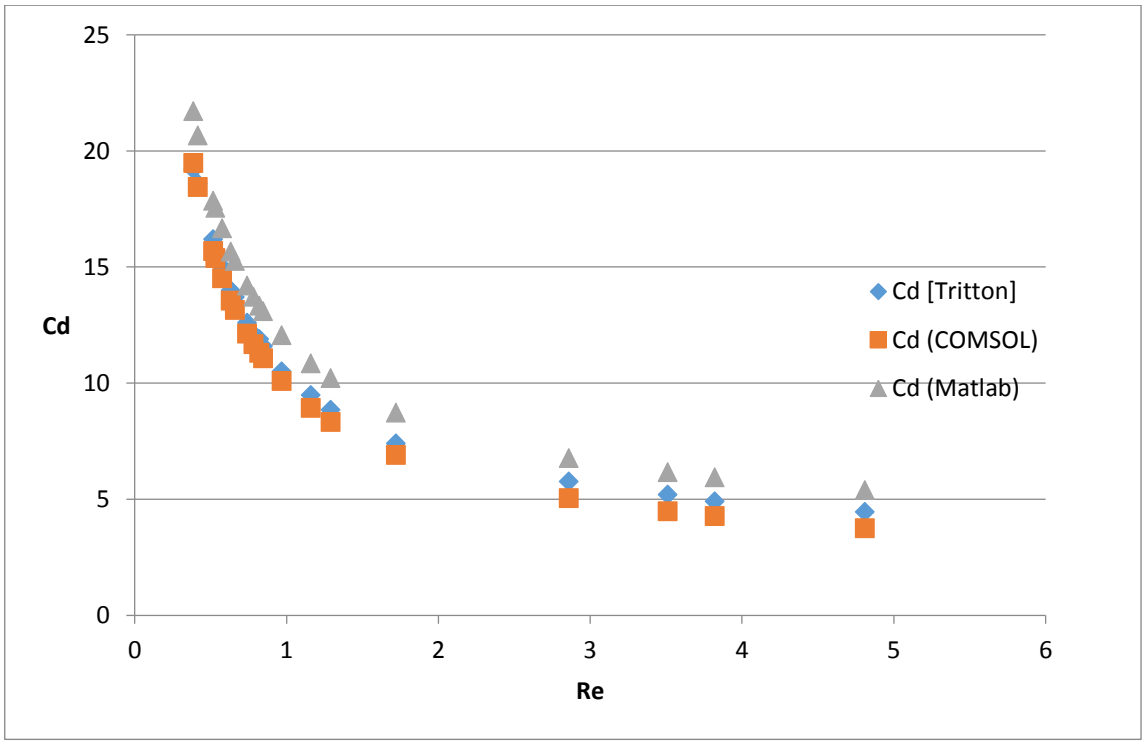

Figure 4.1.1 Visualization of drag coefficient values from COMSOL, Matlab, and experimental data

It can be easily noticed that Cd versus Re plots from experimental data, boundary element method and finite element modelling tools are identical. Even though there is certain offset between the points, the trends are alike.

Table 4.1.1 Drag coefficient comparison

Re	Cd [Tritton]	Cd (COMSOL)	Cd (Matched asymptotic expansion)	Cd (Matlab)	Cd (Analytical solution of Oseen)	Matlab vs Tritton [%]
0,387	19,2	19,47634	19,80546	21,7049	21,7393	13,05
0,416	18,6	18,44772	18,78070	20,6658	20,7001	11,11
0,518	16,2	15,68629	15,99736	17,8559	17,8913	10,22
0,532	15,7	15,38395	15,68922	17,5464	17,5822	11,76
0,576	15,0	14,52198	14,80615	16,6621	16,6990	11,08
0,634	14,0	13,55436	13,80548	15,6658	15,7048	11,90
0,661	13,7	13,15708	13,39122	15,2557	15,2958	11,36
0,741	12,6	12,13596	12,31498	14,1985	14,2427	12,69
0,783	12,1	11,67625	11,82386	13,7213	13,7680	13,40
0,820	11,9	11,30679	11,42545	13,3371	13,3863	12,08
0,845	11,6	11,07378	11,17224	13,0945	13,1455	12,88
0,968	10,5	10,08708	10,07875	12,0648	12,1263	14,90
1,160	9,5	8,92887	8,72864	10,8515	10,9342	14,35
1,290	8,9	8,32212	7,97257	10,2139	10,3147	15,41
1,720	7,4	6,90949	5,92330	8,7251	8,9084	17,75
2,860	5,8	5,05519	0,35888	6,7660	7,3572	17,26
3,510	5,2	4,48355	-5,37779	6,1630	7,0953	18,52
3,820	4,9	4,27079	-9,79314	5,9390	7,0357	20,96
4,810	4,5	3,75197	-44,46146	5,3944	6,5023	21,22

Now, to validate COMSOL model, results from simulations are compared with Tritton's experimental data and matched asymptotic expansion. Comparing drag coefficient values from columns two and three in Table 4.1.1 it can be easily seen that values are close to each other with an average absolute difference equal to 0.5. It is interesting to observe this difference in Figure 4.1.1: COMSOL model is slightly offset from experimental values, but with equal slope all over the testing range. Moreover, COMSOL results are in good agreement with matched asymptotic expansion method up to around Reynolds number Re=1, but then for Re>2,860 the Kaplun's equation yields physically irrelevant values [Yano and Kieda, 1980]. Overall, numbers discussed above are consistent and it can be said that COMSOL is validated. Simultaneously, full Navier-Stokes COMSOL model adds credibility to the Tritton's experiments and used further on.

Thereafter, Oseen integrated Matlab results are going to be validated. Bush presented an analytical solution for the drag coefficient in Oseen's flow and these values are in column six of Table 4.1.1. Comparison of Matlab and analytical solution yields strong evidence that Matlab code works as expected. Then, refer to column seven in Table 4.1 that shows relative difference between Matlab and Tritton's drag coefficient values. There is a fluctuation up to Reynolds number Re=1.16 with highest value being equal to 14.9% difference. After that, a constant divergence over the remaining experimental range of Reynolds number can be observed: at Re=3.82 the difference is already more than 20%. Recall analytical solution of Oseen's equations of motion, where relative difference between Oseen's approximation and Tritton's experiments at low Re is also around 14% [Bush, 1983]. So, the deviation between Matlab and experimental results up to Reynolds number Re=1.16 in Table 4.1 is considered as acceptable.

It was expected that Matlab would start to constantly deviate from empirical data at some point in high Reynolds numbers. In fact, this begins at Re=1.290 with 15.9% relative difference and eventually jumps over 20% benchmark at Re=3.820. Thereby, Matlab code in this study can be reliably used below Reynolds number 1.290.

Summing up this part of the study, it can be said that there is a certain degree of inaccuracy in Oseen integrated Matlab code and further work on its improvement should be done. However, a clear correlation at low Reynolds numbers between COMSOL and matched asymptotic expansion method, Matlab and analytical solution of Oseen, and Tritton experiments leads to the validation of Oseen's approximation in this range. It has been shown that there is a good agreement in drag coefficient values up to Reynolds number Re=1,290. Thus, the underlying theory was developed specifically for low Reynold numbers, and hence, only the corresponding range should be examined.

4.2 Shape optimization

Following the instructions provided for the project, optimization was run with two approaches. Fmincon and GA MATLAB algorithms were launched at particular Reynolds number Re = 0.65 with corresponding initial drag coefficient for the cylinder equal to 15.3776.

As Fmincon requires less time, it was set as initial software and was launched with two different initial points. Those were v = [0.5 0.9 1 1] and v = [0 0 0 0], where v = [B X_b a a_2]. To reach convergence, the simulations took 401 and 258 iterations respectively. Figures 4.2.1 and 4.2.2 show all shapes checked by the program and Figure 4.2.3 shows the finally derived shape.

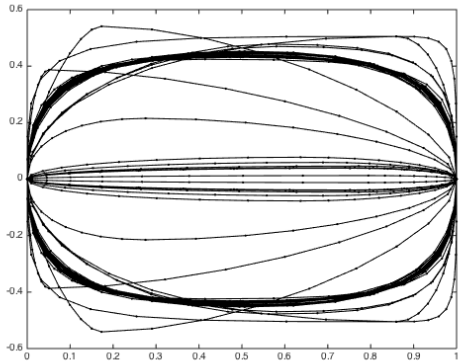

Figure 4.2.1 Fmincon1 generated shapes

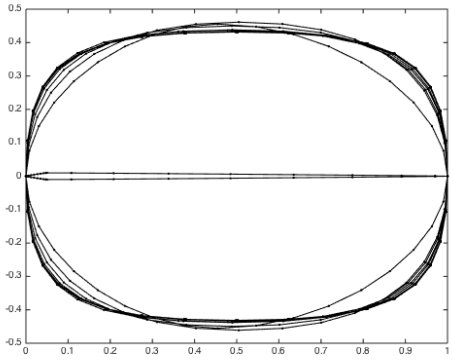

Figure 4.2.2 Fmincon2 generated shapes

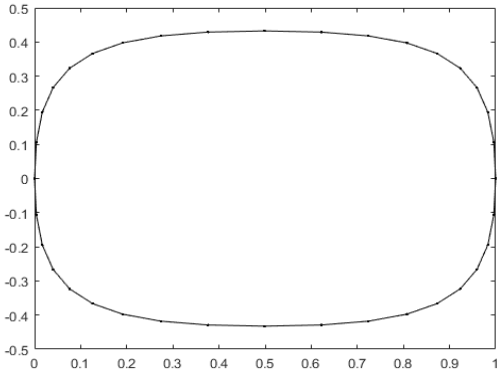

Figure 4.2.3 Final shape from Fmincon1, Fmincon2, Fmincon3 and Fmincon4

Although we started from different initial points, we have achieved, for both cases, almost identical design vectors (final shape parameters). They, taking into account the accuracy of the computation process, provide with some evidence that we have reached the actual minimum drag design. To show some extra verification for the method, relaxed area constraints were launched using previously obtained final shape parameters as initial point, i.e., v = [0.4265 0.4970 0.7779 0.7864]. The two relaxed optimizations (Fmincon3 and Fmincon4) returned equal parameters, which are similar to the previous finding. This provided strong evidence on achieving the necessary results.

Contrary to Fmincon, which takes the source point as the beginning and proceed with further optimization from that point, GA algorithm explores the whole feasible range. It is generally considered as a more robust tool and does not require any initial good guess. In current project it employed the same function constraints as Fmincon and required 7245 iterations to achieve converged results. Its search history is depicted in Figure 4.2.4. As can be seen from Figure 4.2.5, the final resulting shape is different from what was obtained in Fmincon simulation. The resulting parameters satisfy the problem constraints, but the drag result is slightly worse in comparison with Fmincon findings. All simulations were double-checked using COMSOL software and the resulting drag coefficients were verified with a maximum deviation 6.8%. Running GA once more could lead us to a better approximation of the global minimum, but based on the experiments carried out so far, there's strong evidence that the global minimizer has been found by Fmincon. Subsequently, for the current project Fmincon achieved results are selected as the final output and to be accessed to build the modified shape.

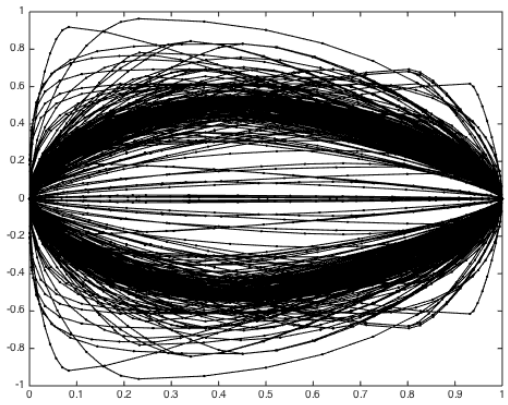

Figure 4.2.4 GA generated shapes

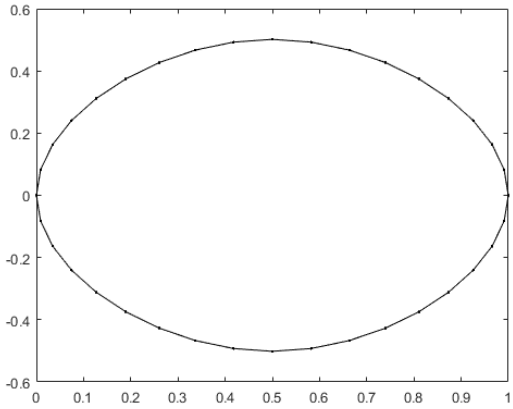

Figure 4.2.5 Final shape from GA

Table 4.2.1 Optimization results

Optimization ID	**V source value [B X_b a a_2]**	**V output value [B X_b a a_2]**	**Drag coefficient from Matlab**	**Drag coefficient from COMSOL**	**Area**	**Area constraint**
Fmincon1	[0.5 0.9 1 1]	[0.4265 0.4970 0.7779 0.7864]	12.1128	12.8437	0.3827	0.01
Fmincon2	[0 0 0 0]	[0.4265 0.4997 0.7811 0.7825]	12.1128	12.7217	0.3827	0.01
Fmincon3	[0.4265 0.4970 0.7779 0.7864]	[0.4267 0.4987 0.7814 0.7799]	12.1126	12.7234	0.3827	0.05
Fmincon4	[0.4265 0.4970 0.7779 0.7864]	[0.4267 0.4987 0.7814 0.7799]	12.1126	12.7234	0.3827	0.1
GA	-	[0.4965 0.4998 0.4399 0.4407]	12.1972	13.0275	0.3816	-

5. Conclusion

In this report a boundary element formulation of Oseen's equations of motion has been used and integrated into MATLAB environment. Two dimensional low Reynolds number flow around a cylinder was examined using the above implementation. Comparison of these drag coefficient values with experimental results from Tritton [Tritton, 1959] and full Navier-Stokes COMSOL simulations showed good agreement up to a Reynolds number of Re=1,290. Even though there was a deviation between the results, relative difference was within the acceptable range and equal to the offset value of analytical technique [Bush, 1983]. Thus, Oseen's equations were validated in aforementioned range of Reynolds numbers and may be used as a sufficient approximation of a true drag. In other cases, i.e., at high Reynolds numbers, full Navier-Stokes equations should be preferred.

Optimization part of the study considered Fmincon and GA algorithms in Matlab to come up with two dimensional shapes that possess minimum drag while retaining the area of the initial shape (circle). The optimized shape exhibits a drag coefficient reduction of 20% while its interior area deviates less than 1% from the initial circular disc.

Reference List

- Brody, J., Yager, P., Goldstein, R. and Austin, R. (1996). Biotechnology at low Reynolds numbers. *Biophysical Journal*, 71(6), pp.3430-3441.
- Bush, M.B. (1983). "Modelling Two-Dimensional Flow Past Arbitrary Cylindrical Bodies Using Boundary Element Formulations". Applied Mathematical Modelling 7 (6): 386-394. Doi:10.1016/0307-904x(83)90142-7.
- Comsol Multiphysics user's guide (2012). Comsol v4.3
- Lagree, P.-Y. (2013), *Small Re flows,* $\varepsilon = Re << 1$.Paris: CNRS and UPMC university
- Olmstead, W. and Gautesen, A. (1976). *Integral representations and the Oseen flow problem*. 1st ed. New York a.o.
- Proudman, I. and Pearson, J. (1957). Expansions at small Reynolds numbers for the flow past a sphere and a circular cylinder. *Journal of Fluid Mechanics*, 2(03), p.237.
- Resnick, A. and Hopfer, U. (2007). Force-Response Considerations in Ciliary Mechanosensation. *Biophysical Journal*, 93(4), pp.1380-1390.
- Rosenstein, Y. and Leshansky, A. (2012). The Oseen problem for a finite collection of spheres settling in a viscous liquid. *European Journal of Mechanics - B/Fluids*, 31, pp.71-79.
- Tritton, D. (1959). Experiments on the flow past a circular cylinder at low Reynolds numbers. *J. Fluid Mech.*, 6(04), p.547.
- Weisenborn, A. and Mazur, P. (1984). The Oseen drag on a circular cylinder revisited. *Physica A: Statistical Mechanics and its Applications*, 123(1), pp.191-208.
- Yano, H. and Kieda, A. (1980). An approximate method for solving two-dimensional low-Reynolds-number flow past arbitrary cylindrical bodies. *J. Fluid Mech.*, 97(01), p.157.

Appendix

A. Stream function calculation for Oseen's approximation by Lagree

Introducing stream function and its expansion, author gets solution of 2D at zero order:

$$\psi = LU_0\bar{\psi} \tag{A.1}$$

$$\psi = \psi_0 + Re\psi_1 + \ldots \tag{A.2}$$

$$\overrightarrow{\overline{\nabla^2}}\overrightarrow{\overline{\nabla^2}}\overline{\psi_0} = 0 \tag{A.3}$$

The challenge here is that no solution of 2D Stoke problem was thought to exist. The good idea would be to try approach from "sphere" model, leading to

$$\overline{\psi_0} = Dsin\theta(2\bar{r}Log(\bar{r}) - \bar{r} + \frac{1}{\bar{r}}) \tag{A.4}$$

The thing is that it is impossible to converge the last equation to zero, which represents the condition at infinity out of the circle. It was lately resolved by starting the problem from the very beginning and takes LU_0 to scale ψ.

$$\frac{\psi_0}{\nu}\left(\left(\frac{\partial\bar{\psi}}{\partial\bar{y}}\frac{\partial}{\partial\bar{x}} - \frac{\partial\bar{\psi}}{\partial\bar{x}}\frac{\partial}{\partial\bar{y}}\right)\overrightarrow{\overline{\nabla^2}}\bar{\psi}\right) = \overrightarrow{\overline{\nabla^2}}\overrightarrow{\overline{\nabla^2}}\bar{\psi} \tag{A.5}$$

The Oseen's problem was defined as far from the body, where viscosity and inertia are playing a role.

$$\psi = \frac{U_0 L}{Re}\breve{\psi}, \quad (x, y) = \frac{L}{Re}(\breve{x}, \breve{y}) \tag{A.6}$$

$$\left(\left(\frac{\partial\breve{\psi}}{\partial\breve{y}}\frac{\partial}{\partial\breve{x}} - \frac{\partial\breve{\psi}}{\partial\breve{x}}\frac{\partial}{\partial\breve{y}}\right)\overrightarrow{\overline{\nabla^2}}\breve{\psi}\right) = \overrightarrow{\overline{\nabla^2}}\overrightarrow{\overline{\nabla^2}}\breve{\psi} \tag{A.7}$$

Then the stream function is expanded to $\breve{\psi} = \breve{y} + \delta\breve{\psi}_1 + \ldots$ with δ unknown yet and the assumption that the flow is nearly not perturbed by the point. Navier-Stokes at order δ

is:

$$\frac{\partial}{\partial \check{x}}\overrightarrow{\overline{\nabla}^2}\check{\psi}_1 = \overrightarrow{\overline{\nabla}}(\overrightarrow{\overline{\nabla}^2}\check{\psi}_1) \tag{A.8}$$

After algebraic manipulations with Goldstein transform, Fourier transform and Euler constant formulation the final solution by Lagree becomes: $\check{\psi} = \frac{1}{Re}(\bar{r}sin\theta + \frac{1}{LogRe}\check{r}(Log(\check{r}) - Log4 + \gamma - 1)$

B. Simulation results

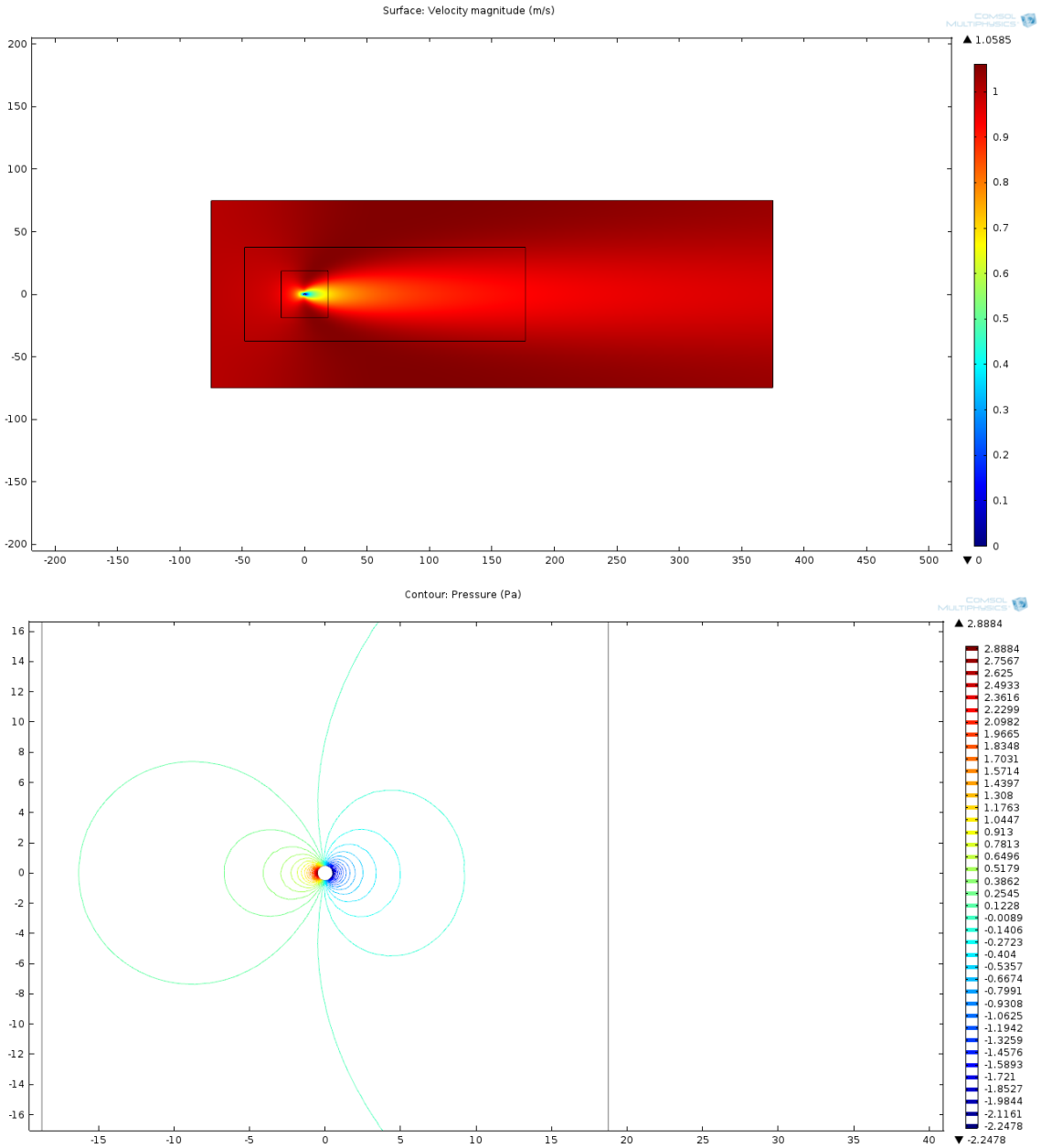

Figure B.1 Velocity and pressure contours at Reynolds number Re=0.532

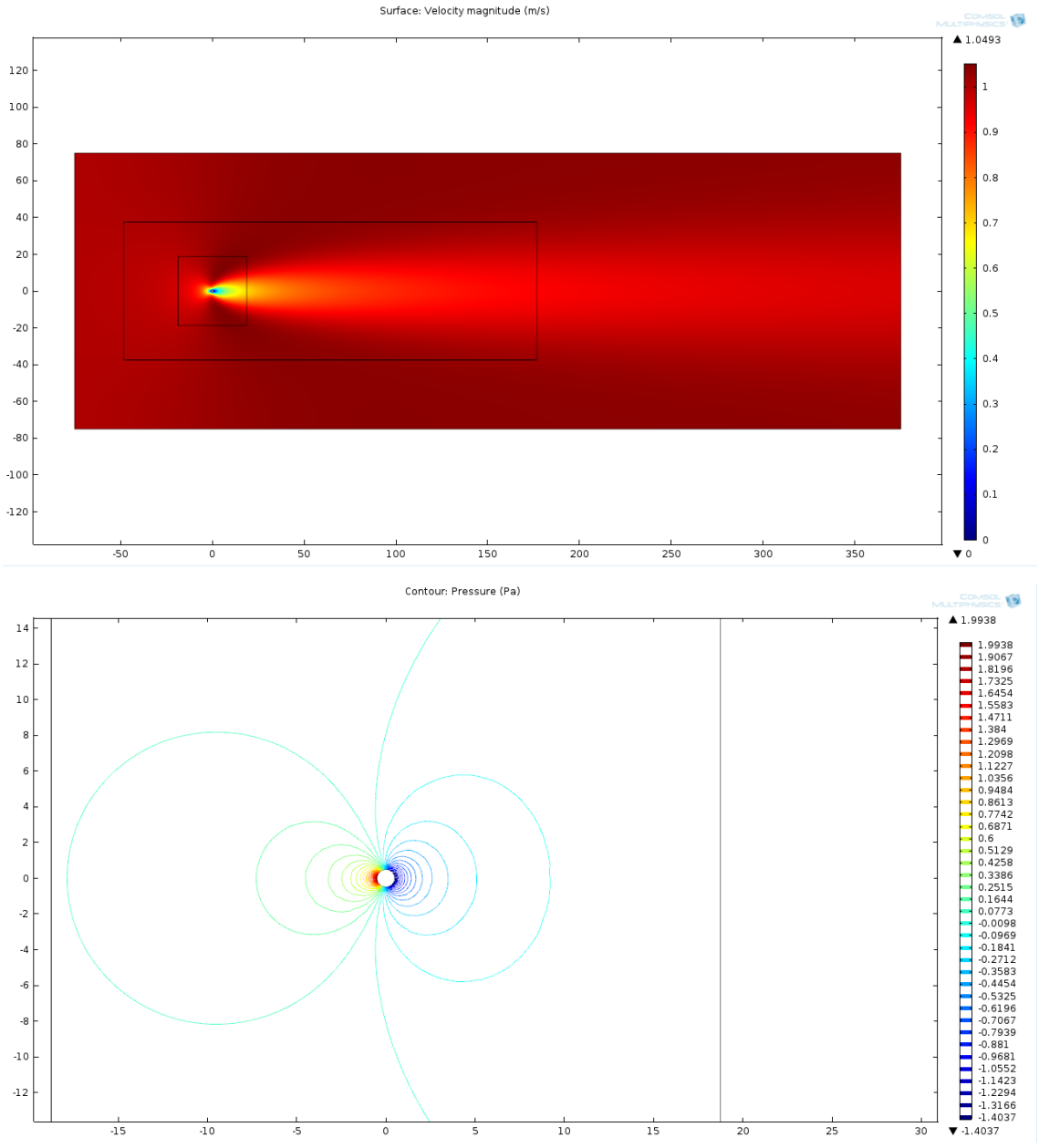

Figure B.2 Velocity and pressure contours at Reynolds number Re=0.968